Closed-Loop Phase Behavior of Polystyrene-*block*-poly(*n*-pentyl methacrylate) Copolymers with Various Block Length Ratios

Du Yeol Ryu,[†] Dong Hyun Lee,[†] Unyong Jeong,[†] Sang-Hyun Yun,[‡] Soojin Park,[§] Kyoon Kwon,[§] Byeong-Hyeok Sohn,[‡] Taihyun Chang,[§] and Jin Kon Kim*,[†]

Departments of Chemical Engineering, Materials Science and Engineering, and Chemistry and Polymer Research Institute, Pohang University of Science and Technology, Kyungbuk 790-784, Korea

Thomas P. Russell

Department of Polymer Science and Engineering, University of Massachusetts, Amherst, Massachusetts 01003

Received February 5, 2004; Revised Manuscript Received March 1, 2004

ABSTRACT: The phase behavior of polystyrene-*block*-poly(*n*-pentyl methacrylate) copolymers [PS−PnPMA] having various block length ratios was investigated by rheology, transmission electron microscopy (TEM), and small-angle X-ray scattering (SAXS). All of the PS−PnPMA exhibited two transitions: the lower disorder-to-order transition (LDOT) and upper order-to-disorder transition (UODT) occurring at a lower and higher temperature, respectively. Thus, PS−PnPMA is characterized by a closed-loop type of phase behavior. As the volume fraction of PS in PS−PnPMA was decreased from 0.5 to 0.23, the microdomains observed between the LDOT and UODT changed from lamellae (LAM) to hexagonally packed cylinders (HEX) and finally to body-centered-cubic spheres (BCC), similar to other block copolymers exhibiting only an order-to-disorder transition. The rheological properties depended strongly on the type of microdomains within the closed-loop. The storage and loss moduli (G' and G'') within the closed loop are the highest for a PS−PnPMA having a BCC morphology, then HEX morphology, and the lowest for LAM morphology.

I. Introduction

Block copolymers have been extensively investigated due to their self-assembly into nanometer-sized morphologies.[1,2] The segregation of the block components due to thermodynamic incompatibility and the connectivity of the two chains produces microdomains of lamella, cylinder, sphere, and gyroid structures.[3−10] Usually, block copolymers exhibit an order-to-disorder transition (ODT) upon heating, where repulsive interaction between constituent segments weakens and phase mixing occurs. A few block copolymers, such as polystyrene-*block*-poly(*n*-alkyl methacrylate) having $n = 2-4$ and polystyrene-*block*-poly(vinyl methyl ether), however, undergo a transition from the phase-mixed to phase-separated state on heating, referred to as the lower disorder-to-order transition (LDOT).[11−15] Here, with increasing temperature the free volume effect arising from differences in thermal expansion coefficients of the blocks becomes greater than the reduction in the enthalpic repulsive interaction.[16,17] Thus, a positive volume change on demixing occurs.[18] Theories on the basis of compressible random phase approximation have been developed to explain the LDOT of block copolymers.[19−25]

Recently, symmetric diblock copolymers of polystyrene-*block*-poly(*n*-pentyl methacrylate) [PS−PnPMA] have been shown to exhibit both an LDOT and an upper order-to-disorder transition (UODT).[26−29] Lamellar microdomains (LAM) were observed between these two transitions, and the copolymers became phase-mixed outside of this temperature range. It is well-known that with a change in the volume fraction of one block (f) in block copolymers from symmetric to asymmetric composition the microdomains change from LAM to hexagonally packed cylinders (HEX) and to body-centered-cubic (BCC) microdomains.[1−5] This general trend of morphology dependence of f is probed for PS−PnPMA having both LDOT and UODT.

Here, phase behavior and morphology of PS−PnPMA were investigated as a function of composition by rheology, transmission electron microscopy (TEM), and small-angle X-ray scattering (SAXS). Asymmetric PS−PnPMAs with HEX or BCC microdomain are shown to exhibit both LDOT and UODT within experimentally accessible temperature range. Thus, PS−PnPMA is characterized by a closed-loop type of phase behavior, within which microdomains depend on the volume fraction of PS in PS−PnPMA.

II. Experimental Section

PS−PnPMAs with various volume fractions of PS block (f_{PS}) were synthesized by the sequential, anionic polymerization of styrene and *n*-pentyl methacrylate in tetrahydrofuran at −78 °C in the presence of LiCl under purified Ar using an *sec*-BuLi initiator.[28] The number- and weight-average molecular weights (M_n and M_w) and the polydispersity index (M_w/M_n) were measured by size exclusion chromatography (SEC) with a multiangle laser light scattering detector. The f_{PS} was determined by nuclear magnetic resonance (NMR), and mass densities were measured at room temperature for the two components (1.05 and 1.03 g/cm^3 for PS and PnPMA, respectively). The molecular characteristics of all PS−PnPMAs are given in Table 1. Only three different values of f_{PS} were used in this study, since transition temperatures corresponding to LDOT and UODT (T_{LDOT} and T_{UODT}) are very sensitive to molecular weight of PS−PnPMA and f_{PS}, as will be discussed later. Only a 10% change in molecular weight changes the transition temperatures by as much as 100 °C.

[†] Department of Chemical Engineering.
[‡] Department of Materials Sciences & Engineering.
[§] Department of Chemistry.
* To whom correspondence should be addressed: e-mail jkkim@postech.ac.kr.

10.1021/ma049746y CCC: $27.50
Published on Web 04/15/2004

Table 1. Molecular Characteristics of PS−PnPMAs Employed in This Study

sample code	M_n	M_w/M_n[a]	f_{PS}[b]	T_{LDOT}[c] (°C)	T_{UODT}[c] (°C)
B-I	46 500	1.02	0.50		
B-IV	49 900	1.02	0.50	142 (141)	220 (222)
B-C1	56 000	1.03	0.39[2]	155 (155)	225 (222)
B-S1	81 600	1.03	0.22[8]	175 (173)	245 (247)

[a] Measured by SEC with a multiangle laser light scattering detector. [b] Measured by nuclear magnetic resonance (NMR). The densities of PS and PnPMA are 1.05 and 1.03 g/cm^3, respectively. [c] Measured by the temperature sweep of G'. The values in parentheses were measured by SAXS experiments. The T_{LDOT} was taken as a starting temperature during the transition, but the T_{UODT} was taken as an end temperature during the transition. The error in determining T_{LDOT} and T_{UODT} was ±1 °C.

An Advanced Rheometric Expansion System (ARES, Rheometrics Co.) with 25 (or 40) mm diameter parallel plates was used to determine the dynamic storage and loss moduli (G' and G'') of PS−PnPMA from 115 to 265 °C at a heating rate of 0.5 °C/min. A strain amplitude (γ_0) of 0.05 and angular frequency (ω) of 0.1 rad/s, which lie in the linear viscoelasticity range, were used. Isothermal frequency sweeps (ω = 0.02−100 rad/s) at γ_0 = 0.05 were performed in step increments of 5 °C. At each temperature, the sample was allowed to thermally equilibrate.

Samples for synchrotron small-angle X-ray scattering (SAXS) measurements were prepared by compression-molding at 115 °C, followed by annealing at 120 °C under vacuum for 24 h. The measurements were performed on Beamline 4C1 and 4C2 at the Pohang Light Source (Korea) where W/B4C double multilayer monochromator delivered monochromatic X-rays onto the samples with a wavelength (λ) of 0.1608 nm and resolution $\Delta\lambda/\lambda \cong 0.01$.[30] A flat Au mirror was used to reject higher harmonics. A 2-D CCD camera (Princeton Instruments Inc., SCX-TE/CCD-1242) was used to collect the scattered X-rays. The sample thickness was 1.5 mm, and the exposure time was 5 min.

Samples for transmission electron microscopy (TEM: JEOL 1200EX electron microscope operating at 120 keV) were prepared by quenching into liquid nitrogen after annealing at a desired temperature. Ultrathin sections were prepared under cryogenic conditions. The PS microdomains of PS−PnPMA copolymers were selectively stained with RuO_4.

III. Results and Discussion

The temperature dependence of G' and G'' is given in Figure 1 for two symmetric PS−PnPMAs upon heating at a rate of 0.5 °C/min. G' and G'' for B-I decreased monotonically with increasing temperature, which is typical for homogeneous molten polymer or a phase-mixed copolymer. This is because the molecular weight of B-I was too low to induce ordered microdomain structure. However, when the molecular weight was slightly increased (∼7%), B-IV was found to undergo two distinct transitions: T_{LDOT} at ∼142 °C and T_{UODT} at 220 °C. Although both transitions were also observed in temporal change of G'', the change of G'' at both transitions was not distinct compared with that of G'. These two transitions can be explained by a delicate balance between enthalpic and entropic contributions to the free energy of mixing.[26−29,31] When the free volume effect prevails, an LDOT is induced. At higher temperatures, translational entropy again prevails over the free volume, which results in the UODT. From Figure 1, it is concluded that T_{LDOT} and T_{UODT} depend strongly on the molecular weight of the block copolymer.

Shown in Figure 2 are frequency sweep measurement for B-I. The slopes of plots of log G' vs log ω and log G'' vs log ω at terminal region are 2 and 1 ($G' \sim \omega^2$, $G'' \sim \omega^1$), respectively. Also, plots of log G' vs log G'' show a temperature independence with a slope of 2 for all temperatures, indicating that B-I becomes disordered in the entire temperature range.

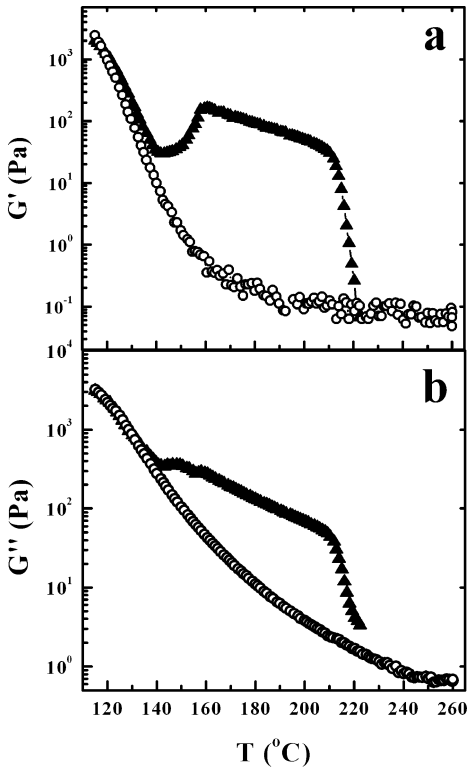

Figure 1. Temperature dependence of (a) G' and (b) G'' for two symmetric PS−PnPMAs: B-I (○) and B-IV (▲).

Figure 3 shows plots of log G' (and log G'') vs log ω and log G' vs log G'' for B-IV. At temperatures lower than 140 °C, the slopes of plots of log G' vs log ω and log G'' vs log ω are 2 and 1, respectively. This suggests that B-IV becomes disordered melt at temperatures lower than 140 °C. However, at lower ω, G' at 145 °C increased by 1 order of magnitude, compared with that at 140 °C. Also, the slope of log G' vs log ω plots was much smaller than 2. This suggests that a transition from disordered to the ordered state occurred near 145 °C. A small slope less than 2 for log G' vs log ω is maintained up to 215 °C. With increasing temperature above 220 °C, G' decreased markedly, indicating that B-IV becomes disordered at temperatures higher than 220 °C. For a disordered block copolymer, plots of log G' vs log G'' do not depend on temperature, and the slope is 2.[8−10] Using this rheological criterion, $T_{LDOT} \sim$ 142 °C and $T_{UODT} \sim$ 220 °C, which is consistent with results shown in Figure 1. It is well-known that for LAM microdomain the transition temperature measured by temporal change in G' is essentially the same as that measured by log G' vs log G'' plots.[10,32] Furthermore, these two values are the same as those obtained by SAXS results as shown in ref 26.

B-IV also exhibits two branches in log G' vs log G'' plots at lower ω: the upper is characteristic of LAM microdomains, and the lower, the disordered state. It should be noted that the data at temperatures lower than T_{LODT} collapse onto the data at temperatures higher than T_{UODT}. Therefore, it can be concluded that, as long as this block copolymer having LAM miscrodomains between LDOT and UODT is disordered, log G' vs log G'' plots do not depend on the temperature.

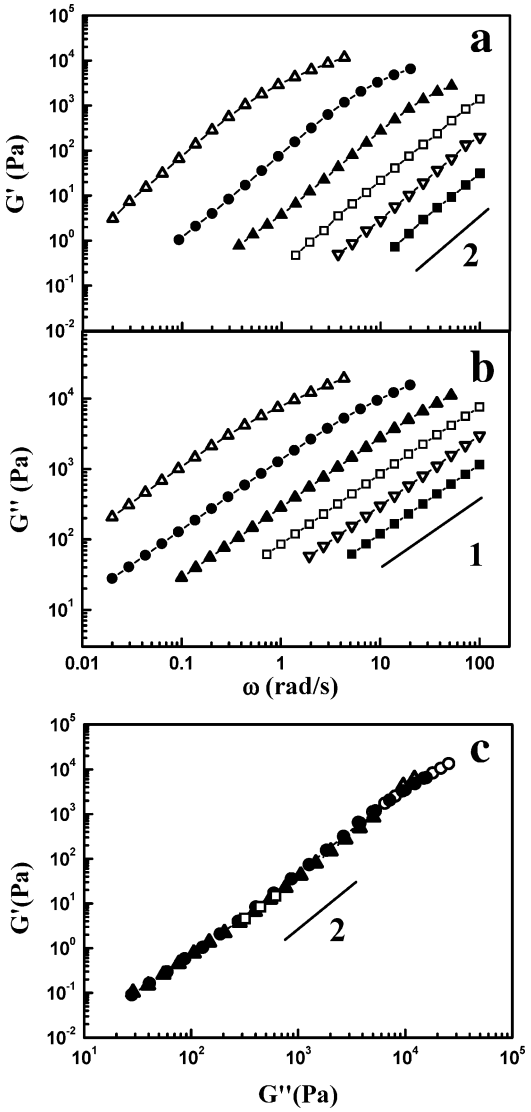

Figure 2. (a) log G' vs log ω plots, (b) log G'' vs log ω plots, and (c) log G' vs log G'' plots for B-I at various temperatures: 130 (△), 150 (●), 170 (▲), 190 (□), 210 (▽), and 230 °C (■).

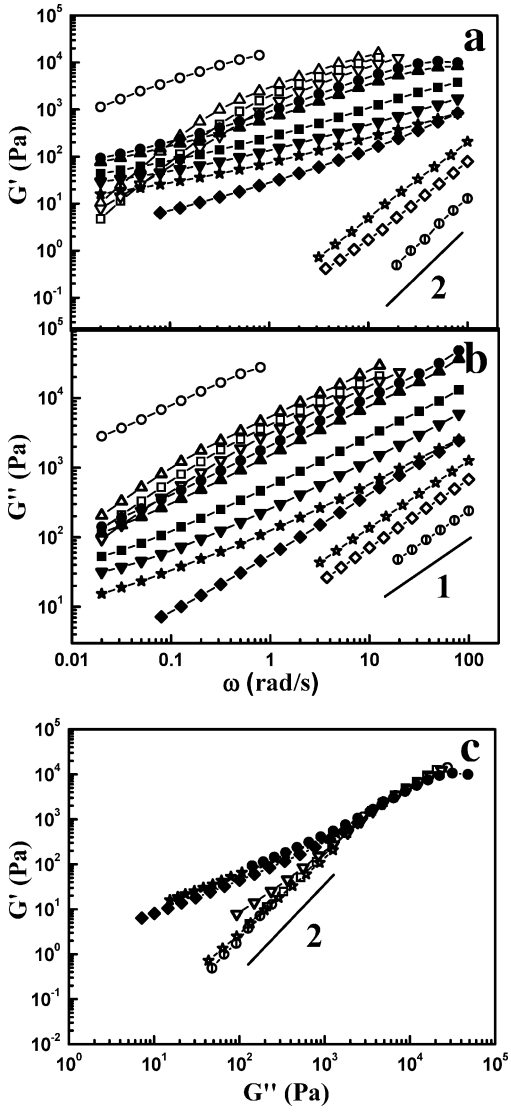

Figure 3. (a) log G' vs log ω plots, (b) log G'' vs log ω plots, and (c) log G' vs log G'' plots for B-IV at various temperatures: 110 (○), 130 (△), 135 (□), 140 (▽), 145 (●), 150 (▲), 170 (■), 190 (▼), 210 (★), 215 (◆), 220 (☆), 230 (◇), and 250 °C (◑).

Thus, a disordered state at temperatures below T_{LDOT} is essentially the same as that at temperatures above the T_{UODT}. This indicates that log G' vs log G'' plots are very useful for determining T_{LDOT} and T_{UODT}.

Figure 4 gives TEM images for B-IV at various temperatures. For sample B-IV to experience the same thermal history employed in Figure 1, temperature was increased from 115 °C to a desired temperature at a rate of 0.5 °C/min. As soon as the temperature reached a desired temperature, the sample was quenched into liquid nitrogen. The TEM images for specimen at both 120 and 240 °C are characteristic of the fluctuation-induced disordered state,[33] which is consistent with rheological measurements. At 142 °C, LAM microdomains begin to appear in the disordered fluctuation. The grains of LAM microdomains become anisotropic, in that the direction parallel to LAM normal is much larger than that perpendicular to LAM normal. This is similar to observations seen in an SI copolymer during the formation of LAM microdomains in the disordered matrix near the ODT.[33] At 180 °C, a TEM image typical of LAM microdomains was seen with a domain spacing of 23 nm. Finally, the dissolution of LAM microdomains into disordered state was seen at 217 °C. Thus, we conclude that T_{LDOT} and T_{UODT} are close to 142 and 217 °C, respectively.

Figure 5 shows the temperature dependence of G' and G'' for B-C1 having $f_{PS} = 0.39$. Similar to the result for B-IV given in Figure 1, with increasing temperature G' and G'' first decrease, but increase markedly at ∼155 °C, then decrease slightly, and finally drop precipitously at 225 °C. Therefore, asymmetric B-C1 shows both an LDOT and UODT at ∼155 and 225 °C, respectively. Since f_{PS} in B-C1 is 0.39, the microdomains between T_{LDOT} and T_{UODT} would be expected to be HEX microdomains, but gyroid microdomains cannot be excluded.

Figure 6a gives a TEM image of B-C1 annealed at 190 °C for 2 days followed by quenching into liquid nitrogen, which clearly shows HEX microdomains. Furthermore, B-C1 exhibited a distinct birefringence, as measured by polarized optical microscopy (POM), between the LDOT and UODT, as shown in Figure 6b. Thus, gyroid microdomains can be completely excluded for B-C1.

Figure 7 shows plots of log G' (and G'') vs log ω and log G' vs log G'' for B-C1. At temperatures lower than

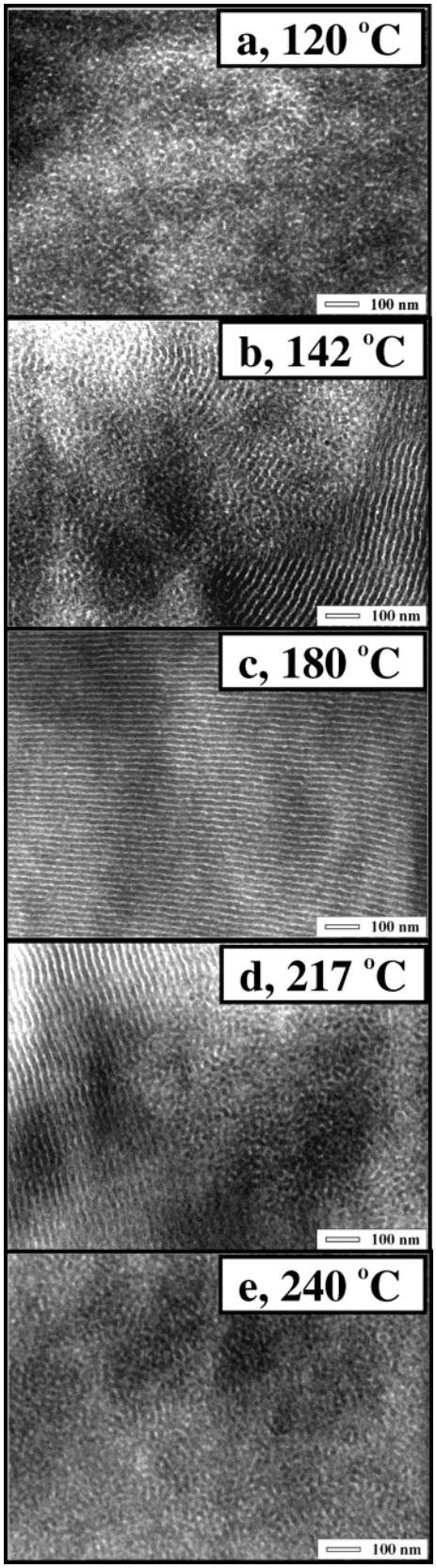

Figure 4. TEM images for B-IV at various temperatures: (a) 120, (b) 142, (c) 180, (d) 217, and (e) 240 °C.

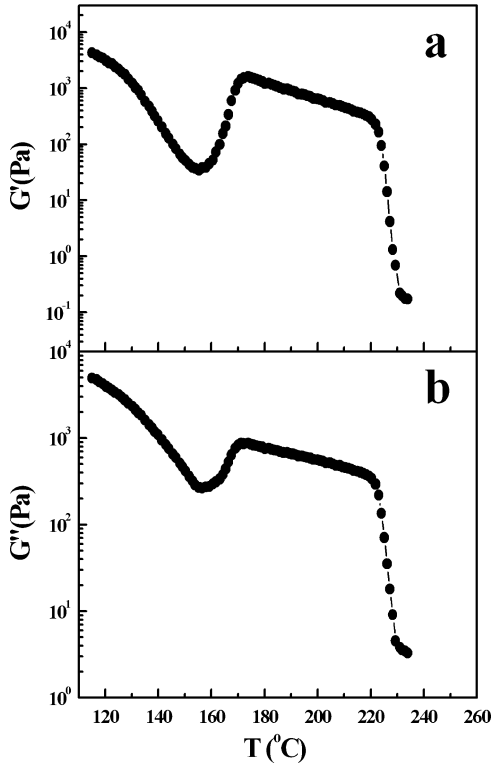

Figure 5. Temperature dependence of (a) G' and (b) G'' for B-C1.

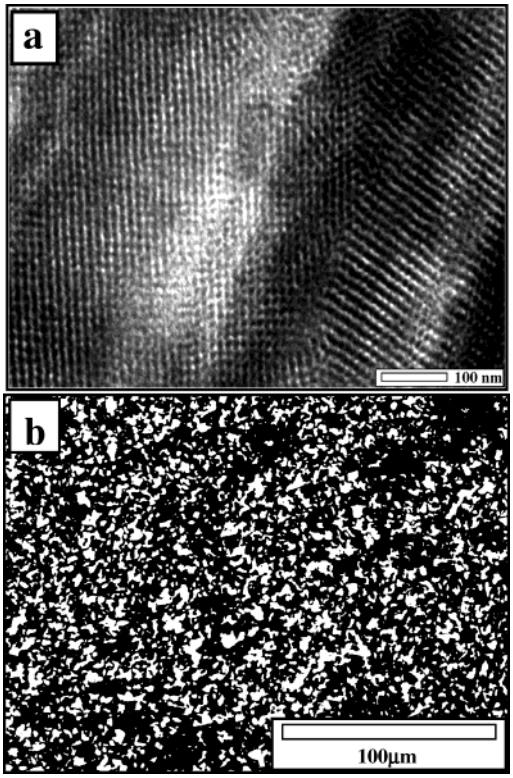

Figure 6. TEM image (a) and POM image (b) for B-C1 measured at room temperature after annealed at 190 °C for 2 days followed by quenched into liquid nitrogen.

150 °C, G' at lower ω decreases with increasing temperature, and the slope of log G' vs log ω plots is 2, indicating that this block copolymer is disordered. Then, G' increased dramatically at ~155 °C. At temperatures between 155 and 220 °C, the slope of log G' vs log ω becomes much smaller than 2. G' at 225 °C decreased significantly, but the slope of log G' vs log ω is still less than 2. At temperatures higher than 230 °C, the slope of log G' vs log ω is again 2. It is seen in Figure 7c that the curve of log G' vs log G'' plots at 155 °C was located at the same curve at 225 °C; T_{LDOT} and T_{UODT} were

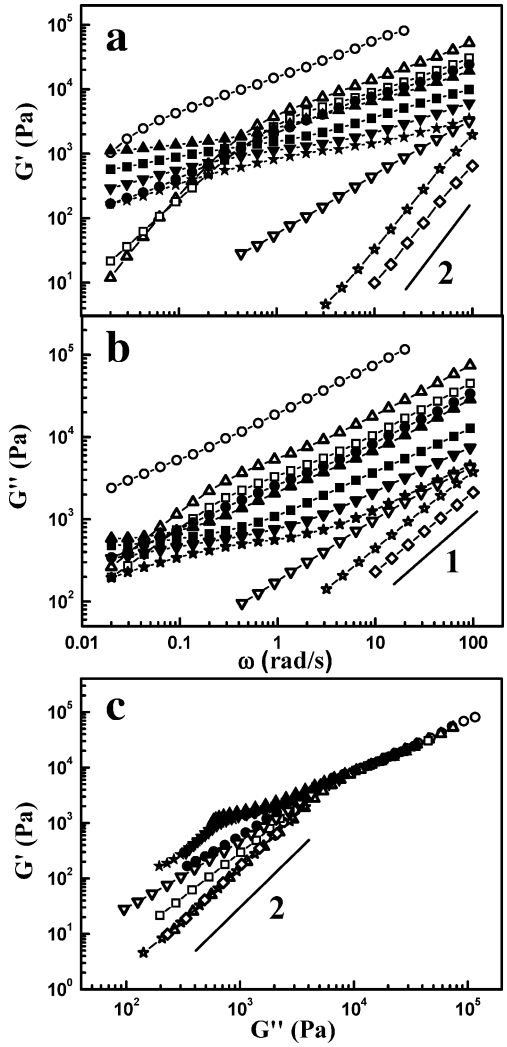

Figure 7. (a) log G' vs log ω plots, (b) log G'' vs log ω plots, and (c) log G' vs log G'' plots for B-C1 at various temperatures: 120 (○), 140 (△), 150 (□), 155 (●), 160 (▲), 180 (■), 200 (▼), 220 (★), 225 (▽), 230 (☆), and 250 °C (◇).

determined to be ∼155 and 225 °C, respectively. The values of T_{LDOT} and T_{UODT} determined from log G' vs log G'' are essentially the same as those obtained from temperature dependence of G' (or G''). Finally, comparing Figure 7 to Figure 3, some differences are evident in the log G' vs log G'' plots in the ordered state. Namely, G' does not decrease steadily with decreasing G'' for B-C1. Rather, when $G'' \sim 7 \times 10^2$ Pa, G' exhibited a small hump. This suggests that the microdomain between LDOT and UODT for B-C1 is different from that for B-IV.

Synchrotron SAXS profiles ($I(q)$ vs q) for B-C1 are shown in Figure 8a as a function of temperature upon heating at a rate of 0.5 °C/min from 120 °C. Here q is the scattering vector ($q = (4\pi/\lambda) \sin \theta$ where 2θ is the scattering angle and λ is the wavelength). At lower temperatures only a broad first-order peak was observed, typical of the correlation hole scattering from a disordered block copolymer. With increasing temperature, the scattering peak sharpens and intensifies, suggesting that this block copolymer undergoes a transition from the disorder to an order states. With further increasing temperature, the scattered intensity decreases again and the block copolymer becomes disordered. A high order peak at $\sqrt{3}q^*$ (in which q^* is the maximum peak position) is barely observed at the SAXS profile even at 190 °C because of very small electron density contrast between PS and PnPMA. However, when the specimen was annealed at 190 °C for 2 days in a vacuum followed by quenching into liquid nitrogen, the SAXS profile taken at room temperature with a

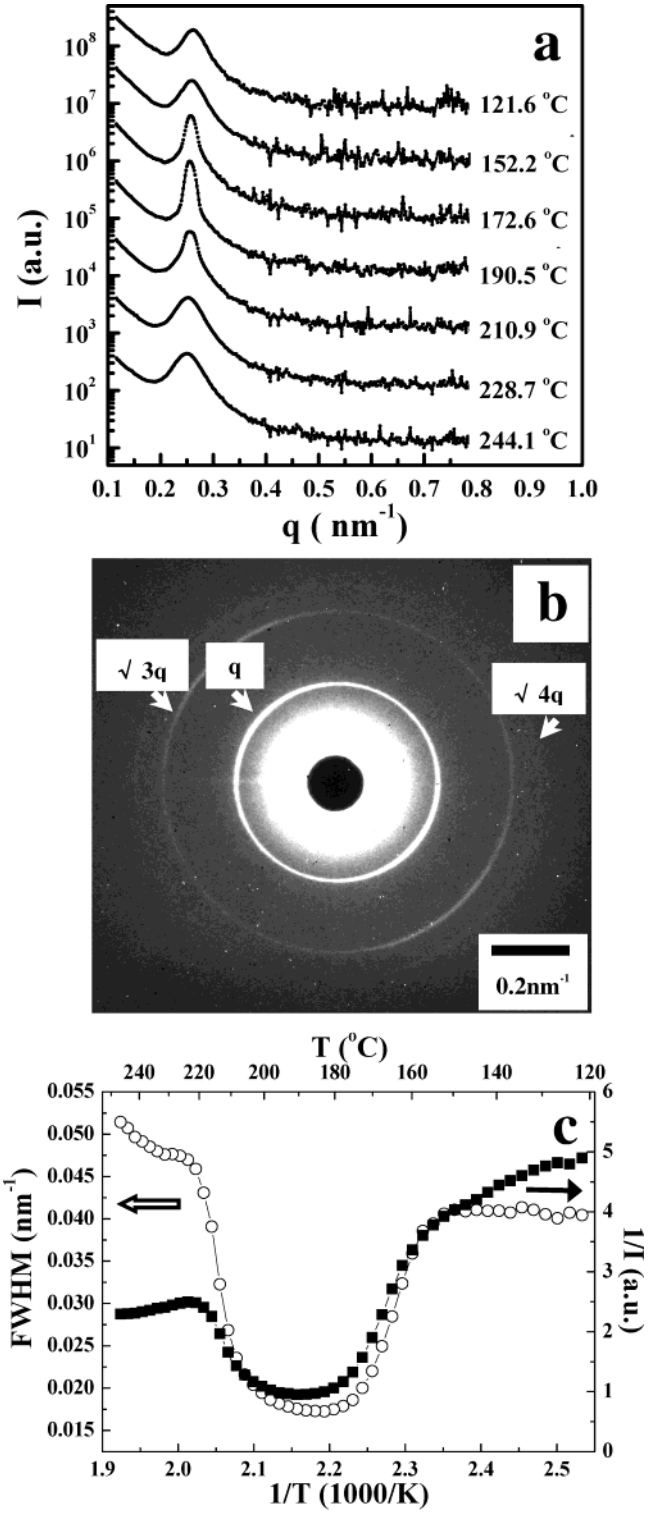

Figure 8. (a) SAXS profiles for B-C1 at various temperatures during heating at a rate of 0.5 °C/min with an exposure time of 2 min. (b) 2-D SAXS image of B-C1 measured at room temperature with a longer exposure time of 10 min after annealing at 190 °C for 2 days in a vacuum followed by quenching into liquid nitrogen. (c) Plots of $1/I_{max}$ (■) and full width at half-maximum (fwhm) (○) vs $1/T$ for B-C1.

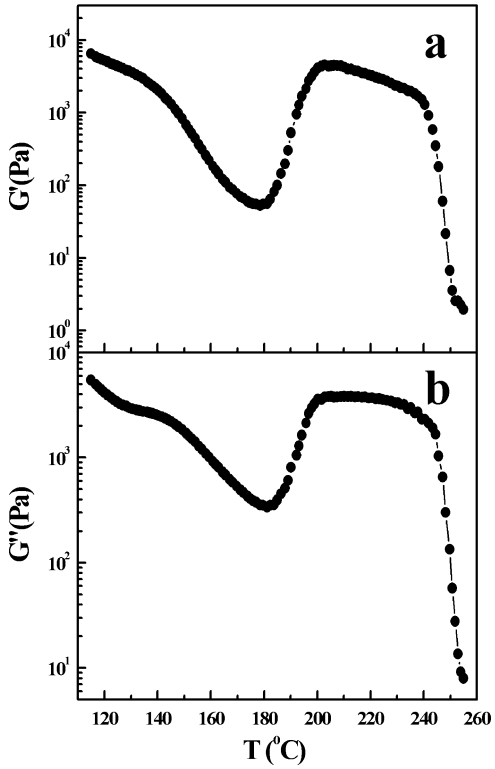

Figure 9. Temperature dependence of (a) G' and (b) G'' for B-S1.

longer exposure time of 10 min clearly exhibited higher-order peaks corresponding to the $\sqrt{3}q^*$ and $\sqrt{4}q^*$, as shown in Figure 8b. Consequently, B-C1 exhibits HEX microdomains for temperatures between T_{LDOT} and T_{UODT}. Plots of the inverse of the maximum intensity ($1/I(q^*)$) and the full width at half-maximum (fwhm) as a function of the inverse temperature ($1/T$) are shown in Figure 8c. Judging from the marked changes of $1/I(q^*)$ and fwhm, the T_{LDOT} and T_{UODT} of PS−PnPMA-C1 are determined to be ∼155 and 222 °C. These two values are consistent with rheological measurements. For all PS−PnPMA employed in this study, the width of the LDOT was a broad (10−20 °C), in comparison to the ∼5 °C width seen in the ODT for incompressible diblock copolymers having LAM or HEX microdomains.

Figure 9 shows the temperature dependence of G' and G'' for B-S1 having $f_{PS} = 0.23$. With increasing temperature, G' and G'' decrease initially. Then these two increase markedly at ∼175 °C and did not decrease much with temperature up to 240 °C, and finally, these drop precipitously at 245 °C. Thus, T_{LDOT} and T_{UODT} were estimated to be ∼175 and 245 °C, respectively. The TEM image of B-S1 annealed at 220 °C for 2 days followed by quenching into liquid nitrogen, as shown in Figure 10, is characteristic of BCC microdomains between the LDOT and UODT. Furthermore, no birefringence was observed, even when the sample was annealed for 3 h at a temperature between T_{LDOT} and T_{UODT}. This excludes completely the existence of HEX microdomains in B-S1.

Figure 11 gives plots of log G' (and log G'') vs log ω and log G' vs log G'' for B-S1 at various temperatures. At temperatures lower than 170 °C, B-S1 exhibited rheological properties which are typical for the disordered state. From plots of log G' vs log ω, the T_{LDOT} and T_{UODT} are determined to be ∼175 and 245 °C, respectively. At temperatures between the two transitions, G' does not change for large range of ω in plots of log G' vs log ω, which is typical for BCC microdomains.[34] Furthermore, a negative slope in log G' and log G'' plots at temperatures between T_{LDOT} and T_{UODT} was observed. This is further evidence of BCC microdomains, as demonstrated previously by Han and co-workers.[35,36] Finally, log G' vs log G'' plots become temperature-independent at temperatures higher than 260 °C. Also, these plots become temperature-independent between 120 and 170 °C. Interestingly, the curves at 260 and 270 °C are located slightly lower than between 120 and 170 °C, as shown in the inset of Figure 11. This behavior is different behavior observed in PS−PnPMAs with LAM and HEX microdomains where the curves in log G' vs log G'' at temperatures below the LDOT and above UODT superimpose (see Figures 3 and 7). Although this behavior observed for B-S1 is not understood clearly, it might be attributed to the existence of disordered micelles in the disordered state when BCC microdomains become disordered homogeneous state.[37] Also, two disordered states (namely, a disorder at temperatures lower than T_{LODT} and another one at temperatures higher than T_{UODT}) might have different temperature ranges for the existence of disordered micelles. This speculation is under investigation by using a highly asymmetric PS−PnPMA with $f_{PS} \sim 0.1$.

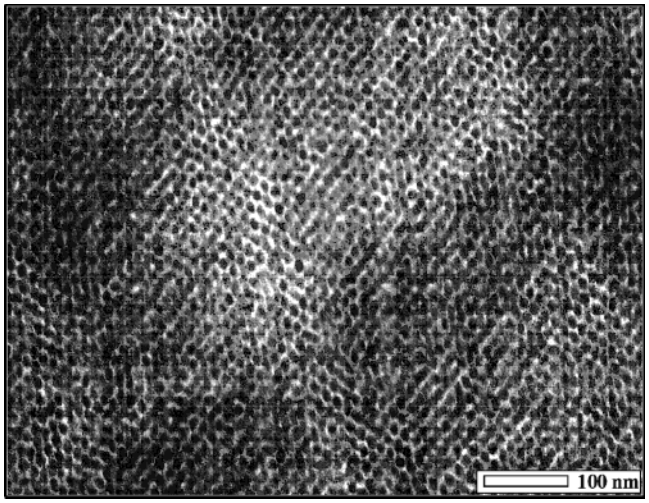

Figure 10. TEM images for B-S1 after annealed at 220 °C for 2 days followed by quenched into liquid nitrogen.

Figure 12a gives SAXS profiles at various temperatures for B-S1. At temperatures lower than 175 °C, a broad peak is observed, suggesting that this block copolymer is disordered. With increasing temperature, sharp and intense scattered peaks are observed, characteristic of an ordered block copolymer. At higher temperature than 245 °C, a disordered state is again observed for SAXS profiles. In the ordered state, SAXS profiles showed higher ordered peaks at $\sqrt{2}q^*$, $\sqrt{3}q^*$, and $\sqrt{4}q^*$, although these peaks are small. Of course, when a specimen was annealed at 220 °C for 2 days followed by quenching into liquid nitrogen, SAXS profile measured at room temperature with a longer exposure time of 10 min showed distinct higher-order peaks, as shown in Figure 12b, indicating that that B-S1 exhibited BCC microdomains. On the basis of SAXS profiles, plots of $1/I(q^*)$ and the fwhm vs $1/T$ are given in Figure 12c. From these data, the T_{LDOT} and T_{UODT} were estimated to be 173 and 247 °C, respectively, which is consistent with rheological measurements.

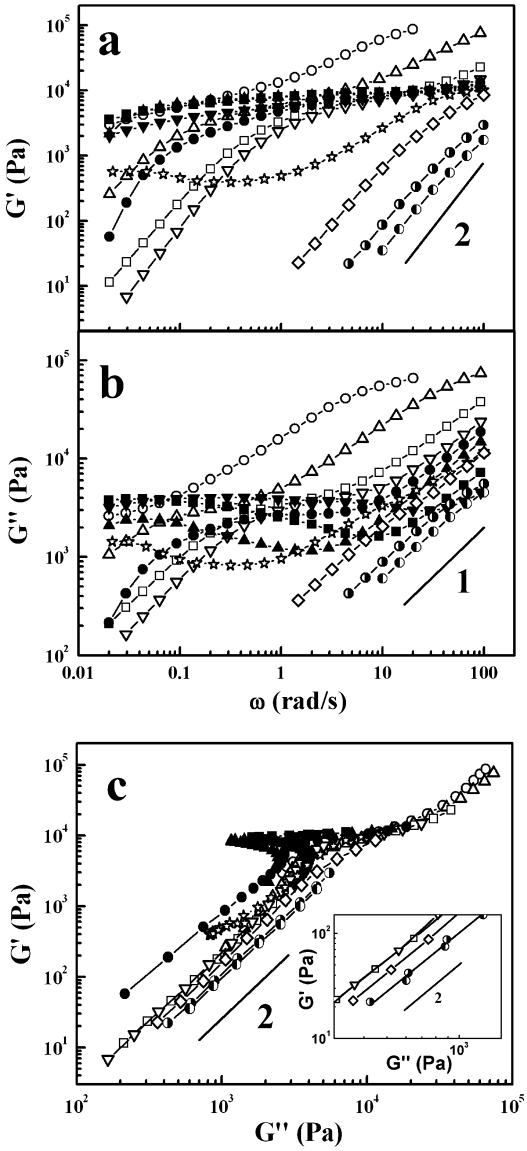

Figure 11. (a) log G' vs log ω plots, (b) log G'' vs log ω plots, and (c) log G' vs log G'' plots for B-S1 at various temperatures: 120 (○), 140 (△), 160 (□), 170 (▽),175 (●), 180 (▲), 200 (■), 220 (▼), 245 (☆), 250 (◇), 260 (◑), and 270 °C (◐).

Finally, we considered the values of G' and G'' of three different ordered states (LAM, HEX, and BCC). The plateau value of G's at ordered state was the largest for BCC microdomains, HEX, and then the smallest for LAM microdomains. G' has been reported to increase with increasing structural dimensions of microdomains.[38−40] Since the dimensions of LAM, HEX, and BCC increase from 1 to 3, this is consistent with the results reported here.

Interestingly, G' of B-S1 exhibited a plateau value (∼5 × 10^3 Pa) between 200 ∼230 °C, as shown in Figure 11. Kossuth et al.[34] showed that the plateau value (G^0_{cubic}) of various diblock copolymers having cubic phases of BCC and gyroid microdomains is directly related to the characteristic domain spacing (d^*) of cubic phases. Using Figure 12 of ref 34 with a value of $d^* \sim$ 28 nm for PS−PnPMA having BCC microdomains, G^0_{cubic}/RT for PS−PnPMA was estimated to be ∼1.5 (thus, estimated G^0_{cubic} at 220 °C is ∼6 × 10^4 Pa, which is close to the experimental value). Therefore, the relationship of $G^0_{cubic}/RT \sim (d^*)^{-3.14}$ in ref 34 would be

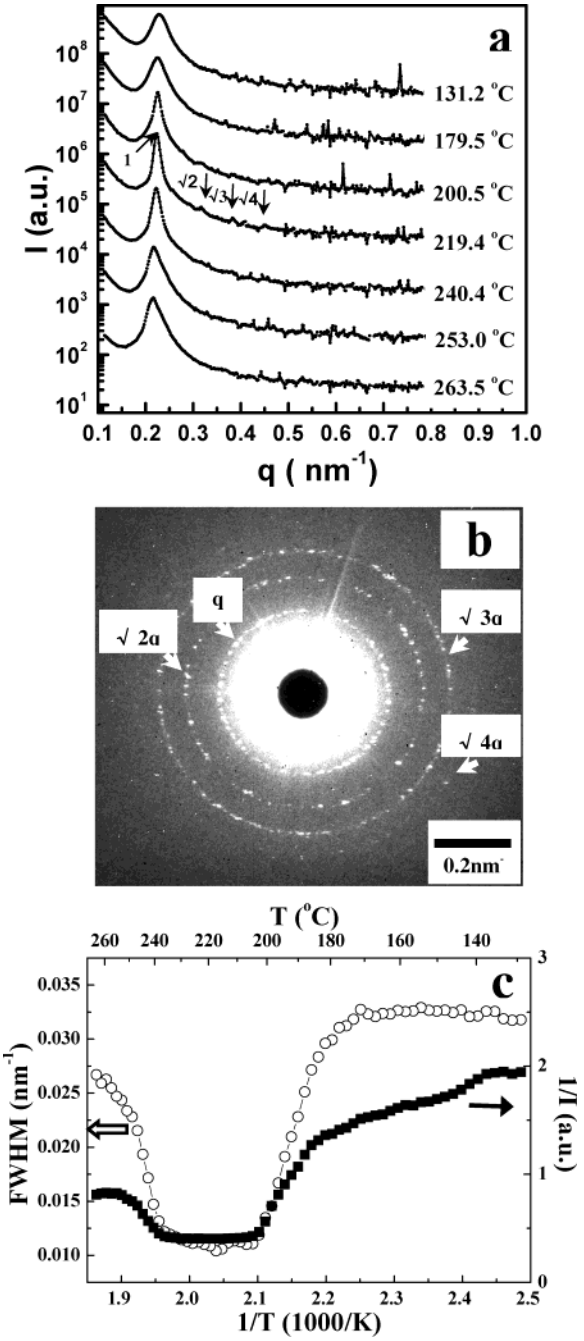

Figure 12. (a) SAXS profiles for B-S1 at various temperatures during heating at a rate of 0.5 °C/min with an exposure time of 2 min. (b) 2-D SAXS image of B-C1 measured at room temperature with a longer exposure time of 10 min after annealing at 220 °C for 2 days in a vacuum followed by quenching into liquid nitrogen. (c) Plots of $1/I_{max}$ (■) and fwhm (○) vs $1/T$ for B-C1.

valid to predict G^0_{cubic} even for PS−PnPMA having a closed-loop phase behavior, and a plateau value of G' of a block copolymer having BCC microdomains might not change much with chemical structures of constituents of block copolymers or types of phase behavior.

IV. Concluding Remarks

In this study, we have shown, via rheology, TEM, and SAXS, that two transitions, an LDOT and UODT, were observed for PS−PnPMA regardless of block length ratios as long as the molecular weight and f_{PS} are properly chosen. Within the two transitions, the micro-

domains changed from lamellar (LAM) to hexagonally packed cylindrical (HEX) and finally to body-centered-cubic spherical (BCC) microdomains, with decreasing f_{PS} from 0.5 to 0.23.

The rheological properties depended on the nature of the microdomains within the closed-loop. The values of G' and G'' at temperatures within the closed loop are the largest for a PS−PnPMA having BCC, then PS−PnPMA having HEX, and the smallest for PS−PnPMA having LAM microdomains. When PS−PnPMA is disordered at temperatures lower than T_{LODT} and higher than T_{UODT}, $G' \sim \omega^2$ and $G'' \sim \omega$ regardless of block length ratios.

Acknowledgment. This work was supported by the POSTECH Research Fund (2003) and by the National RND Project for Nano Science and Technology (M1-0214-00-0230). D.Y.R. is thankful for the Post-doctoral Fellowship program of KOSEF, and T.C. acknowledges the support from KOSEF (Center for Integrated Molecular Systems). Small-angle X-ray scattering (4C1 and 4C2) was performed at PLS beamline supported by POSCO and KOSEF.

References and Notes

(1) Hashimoto, T. In *Thermoplastic Elastomers*; Legge, N. R., Holden, G., Schroeder, H. E., Eds.; Hanser: New York, 1987.
(2) Bates, F. S.; Fredrickson, G. H. *Annu. Rev. Phys. Chem.* **1990**, *41*, 525.
(3) Helfand, E.; Wasserman, Z. R. In *Developments in Block Copolymer*; Goodman, I., Ed.; Applied Science: New York, 1982; Chapter 4.
(4) Leibler, L. *Macromolecules* **1980**, *13*, 1602.
(5) Matsen, M. W.; Bates, F. S. *Macromolecules* **1996**, *29*, 1091.
(6) Bates, F. S. *Macromolecules* **1984**, *17*, 2607.
(7) Fredrickson, G. H.; Bates, F. S. *Annu. Rev. Mater. Sci.* **1996**, *26*, 501.
(8) Han, C. D.; Kim, J.; Kim, J. K. *Macromolecules* **1989**, *22*, 383.
(9) Han, C. D.; Baek, D. M.; Kim, J. K. *Macromolecules* **1990**, *23*, 561.
(10) Han, C. D.; Baek, D. M.; Kim, J. K.; Ogawa, T.; Hashimoto, T. *Macromolecules* **1995**, *28*, 5043.
(11) Russell, T. P.; Karis, T. E.; Gallot, Y.; Mayes, A. M. *Nature (London)* **1994**, *368*, 729.
(12) Ruzette, A. V. G.; Banerjee, P.; Mayes, A. M.; Pollard, M.; Russell, T. P.; Jerome, R.; Slawecki, T.; Hjelm, R.; Thiyagarajan, P. *Macromolecules* **1998**, *31*, 8509.
(13) Weidisch, R.; Stamm, M.; Schubert, D. W.; Arnold, M.; Budde, H.; Horing, S. *Macromolecules* **1999**, *32*, 3405.
(14) Hashimoto, T.; Hasegawa, H.; Hashimoto, T.; Katayama, H.; Kamigaito, M.; Sawamoto, M.; Imai, M. *Macromolecules* **1997**, *30*, 6819.
(15) Hasegawa, H.; Sakamoto, N.; Takeno, H.; Jinnai, H.; Hashimoto, T.; Schwahn, D.; Frielinghaus, H.; Janben, S.; Imai, M.; Mortensen, K. *J. Phys. Chem. Solids* **1999**, *60*, 1307−1312.
(16) McMaster, L. P. *Macromolecules* **1973**, *6*, 760.
(17) Patterson, D.; Robard, A. *Macromolecules* **1978**, *11*, 690.
(18) Pollard, M.; Russell, T. P.; Ruzette, A. V. G.; Mayes, A. M.; Gallot, Y. *Macromolecules* **1998**, *31*, 6493.
(19) Dudowicz, J.; Freed, K. F. *Macromolecules* **1991**, *24*, 5076.
(20) Dudowicz, J.; Freed, K. F. *Macromolecules* **1993**, *26*, 213.
(21) Dudowicz, J.; Freed, K. F. *Macromolecules* **2000**, *33*, 5292.
(22) Yeung, C.; Desai, R. C.; Shi, A. C.; Noolandi, J. *Phys. Rev. Lett.* **1994**, *72*, 1834.
(23) Hino, T.; Prausnitz, J. M. *Macromolecules* **1998**, *31*, 2636.
(24) Cho, J. *Macromolecules* **2000**, *33*, 2228; **2001**, *34*, 1001.
(25) Ruzette, A. V. G.; Mayes, A. *Macromolecules* **2001**, *34*, 1894.
(26) Ryu, D. Y.; Jeong, U.; Kim, J. K.; Russell, T. P. *Nature Mater.* **2002**, *1*, 114.
(27) Ryu, D. Y.; Park, M. S.; Chae, S. H.; Jang, J.; Kim, J. K.; Russell, T. P. *Macromolecules* **2002**, *35*, 8676.
(28) Ryu, D. Y.; Jeong, U.; Lee, D. H.; Kim, J.; Youn, H. S.; Kim, J. K. *Macromolecules* **2003**, *36*, 2894.
(29) Ryu, D. Y.; Lee, D. J.; Kim, J. K.; Lavery, K. A.; Russell, T. P.; Han, Y. S.; Sung, B. S.; Lee, C. H.; Thiyagarajan, P. *Phys. Rev. Lett.* **2003**, *90*, 235501.
(30) Bolze, J.; Kim, J.; Huang, J.; Rah, S.; Youn, H. S.; Lee, B.; Shin, T. J.; Ree, M. *Macromol. Res.* **2002**, *10*, 2.
(31) Ruzette, A. V. G. *Nature Mater.* **2002**, *1*, 85.
(32) Choi, S.; Vaidya, N. Y.; Han, C. D.; Sota, N.; Hashimoto, T. *Macromolecules* **2003**, *36*, 7707.
(33) Sakamoto, N.; Hashimoto, T. *Macromolecules* **1998**, *31*, 3815.
(34) Kossuth, M. B.; Morse, D. C.; Bates, F. S. *J. Rheol.* **1999**, *43*, 167.
(35) Sakamoto, N.; Hashimoto, T.; Han, C. D.; Kim, D.; Vaidya, N. Y. *Macromolecules* **1997**, *30*, 1621, 5321.
(36) Han, C. D.; Vaidya, N. Y.; Kim, D.; Shin, G.; Yamaguchi, D.; Hashimoto, T. *Macromolecules* **2000**, *33*, 3767.
(37) Choi, S.; Lee, K. M.; Han, C. D.; Sota, N.; Hashimoto, T. *Macromolecules* **2003**, *36*, 793.
(38) Ryu, C. Y.; Lee, M. S.; Hajduk, D. A.; Lodge, T. *J. Polym. Sci., Polym. Phys. Ed.* **1997**, *35*, 2811.
(39) Kim, J. K.; Lee, H. H.; Gu, Q.; Chang, T.; Jeong, Y. H. *Macromolecules* **1998**, *31*, 4045.
(40) Jeong, U.; Lee, H. H.; Yang, H.; Kim, J. K.; Okamoto, S.; Aida, S.; Sakurai, S. *Macromolecules* **2003**, *36*, 1685.

MA049746Y